Porewater exchange drives trace metal, dissolved organic carbon and total dissolved nitrogen export from a temperate mangrove wetland

Mahmood Sadat-Noori and William Glamore

Water Research Laboratory, School of Civil & Environmental Engineering, UNSW Sydney, NSW 2052, Australia

Corresponding author:

M. Sadat-Noori, Water Research Laboratory, School of Civil & Environmental Engineering, University of New South Wales,110 King St., Manly Vale, NSW, 2093, Australia

Email: m.sadat-noori@unsw.edu.au; Tel: (+61) 2 80710 9879

Abstract

Porewater exchange is usually the least quantified process in delivering dissolved material from wetlands to coastal waters, although it has been recognised as an important pathway for the transport of trace metal, carbon and nutrient to the ocean. Here, surface water export fluxes of dissolved manganese (Mn), iron (Fe), dissolved organic/inorganic carbon (DOC/DIC), total dissolved nitrogen (TDN) and phosphorous (TDP) were estimated from a temperate mangrove wetland (Kooragang Island, Newcastle, Australia). Radon (^{222}Rn, a natural groundwater tracer) was used to develop a mass balance model to quantify porewater exchange rates and evaluate the porewater-derived dissolved material contribution to the overall wetland export. A 25-h time series dataset depicted a clear peak of Mn, Fe, TDN, DOC and radon during ebb tides which related to porewater discharge. Porewater exchange rates were estimated to be 14.0 ± 6.3 cm/d (0.18 ± 0.08 m^3/s), mainly driven by tidal pumping, and facilitated by a large number of crab burrows at the site. Results showed that the wetland was a source of Mn, Fe, TDN and DOC to the adjacent river system and a sink for TDP and DIC. Surface water Mn, Fe, TDN and DOC exports were 4.0 ± 0.6, 6.6 ± 1.6, 23.9 ± 3.6 and 197.7 ± 29.7 mmol/m^2 wetland/d, respectively. Porewater-derived Mn, Fe, TDN and DOC accounted for ~ 95, 100, 89 and 54% of the wetland surface water exports demonstrating its significant contribution. Our study indicates that temperate mangrove wetlands can be a major source of dissolved metal, carbon and nutrient delivery to coastal waters and that mangrove porewater exchange significantly contributes to this process.

Keyword: wetland hydrology, radon, submarine groundwater discharge, nutrient, estuary, Hunter River.

Introduction

Mangrove wetlands with inter-tidal estuarine systems, are highly productive coastal environments worldwide despite occupying less than 1% of the worlds surface area (Dittmar et al., 2006). Mangrove wetlands, whether modified or pristine, have the capacity to store large amount of metal, carbon and nutrient in their sediments (Wang et al., 2019; Thanh-Nho et al., 2019; Sanders et al., 2014). Due to the low rates of material transformation and retention, these systems can export large volumes of dissolved material to coastal waters (Taillardat et al., 2018; Tait et al., 2017). In particular, mangrove wetlands with small catchments and short residence times have shown to play a disproportionate role in exporting dissolved material compared to some larger riverine systems on a catchment area basis (Call et al., 2019; Holloway et al., 2016; Sadat-Noori et al., 2016a). While many processes contribute to cause this large material export from mangrove wetlands, groundwater discharge and/or porewater exchange is probably the most poorly resolved component and has received limited attention until recently (Webb et al., 2019).

Submarine groundwater discharge (SGD) and/or porewater exchange is defined as any flow of water from sediments to surface waters regardless of its composition, magnitude and scale (Burnett et al., 2003). SGD can originate from deep or shallow aquifers and is usually driven by the hydraulic gradient, tidal pumping and density driven water convection that occurs over various temporal and spatial scales (Santos et al., 2012a). SGD can play a major role in water budgets within catchments (Zhou et al., 2019) and be a significant pathway for solute and dissolved material transport directly to the coastal zone or to streams discharging in the immediate coastal aquatic environment (David et al., 2019; Adyasari et al., 2019; Diggle et al., 2019; Cho et al., 2018; Goodridge, 2018). However, due to SGDs large spatial and temporal variability, quantifying SGD/porewater exchange in aquatic systems remains a challenge and therefore, is usually overlooked in coastal trace metal, carbon and nutrient budgets.

Natural geochemical tracers, such as radon (^{222}Rn), are effective tools for assessing SGD both qualitatively and quantitatively and can overcome some inherent challenges associated with SGD/porewater exchange studies (Peterson et al., 2019; Webb et al., 2019). Radon is a noble gas with low chemical reactivity and has a half-life of 3.8 days that is on the same temporal scale as most physical processes that (typically) drive SGD in coastal environments (Burnett et al., 2008). Another advantage of radon is that measuring radon at one point (usually the outlet of the catchment) integrates the radon signal coming from various SGD pathways, which accounts for the spatial heterogeneity of the catchment (Burnett et al., 2006). These

properties make radon an ideal tool for evaluating SGD in coastal environments where often hydraulic conductivity, transmissivity and aquifer thickness information may not be available to develop conventional groundwater flow models.

Previous studies have reported that SGD/porewater exchange can be a major driver of trace metal (Holloway et al., 2016), carbon dynamics (Webb et el., 2019) and nutrient (Tait et al., 2017), in mangrove wetlands, making SGD/porewater exchange an important driver of biogeochemical cycles in coastal waters (Moore, 2010; Moore 2006). However, most previous studies focused on mangroves in tropical and subtropical climates and less information is available on porewater-derived solutes in temperate mangrove systems. In this study we build on the available literature by quantifying porewater-derived dissolved manganese (Mn), iron (Fe), dissolved inorganic carbon (DIC), dissolved organic carbon (DOC), total dissolved nitrogen (TDN) and total dissolved phosphorus (TDP) fluxes from a temperate mangrove wetland in Southeast Australia. Radon is used to estimate temporal variability of porewater exchange rates at the tidal wetland. Associated material fluxes over a full diel cycle are calculated to determine the overall lateral export of trace metal, carbon and nutrient from the wetland during a non-flood period. Additionally, nutrients and carbon delivered to the coastal ocean through mangrove porewater is compared with nutrients and carbon transported by the adjacent river to highlight the relative importance of porewater exchange.

Material and Methods

Study Site

Field investigations were carried out in a coastal temperate mangrove wetland located at Kooragang Island (-32.866707S, 151.715561E), approximately 10 km upstream of the oceanic entrance of the Hunter River Estuary, Newcastle, Australia (Figure 1). The wetland has a small catchment of 24 ha, is low-lying, which reduces surface water drainage, and has no upstream freshwater inputs. The area experiences a temperate climate and receives 1122 mm of accumulated rainfall, on average, annually. Temperatures at the site range from 18 to 27 °C in summer (December to February) and 7 to 17 °C in winter (June – August) (Bureau of Meteorology; http://www.bom.gov.au). The wetland has an estuarine channel discharging to the Hunter River known as Fish Fry Creek, which is 170 m long and 10 m wide. The channel connects the entrance to the intertidal mudflats which cover an area of 112,450 m^2. The

overbank wetland area is tidally dominated, characterised by a semidiurnal tidal regime with spring and neap tides ranging from 0.7 to 2 m.

Experimental approach

The experimental approach consisted of 1) surface water time series grab samples collected for dissolved trace metal, carbon and nutrient over a 25-hour time period to cover a full diel cycle (two tidal cycles) and processes occurring in surface water; 2) porewater sampling within the wetland to characterise the composition of the end-member elements; 3) quantification of porewater exchange at the wetland using a radon mass balance approach; 4) combining the above to estimate the contribution of porewater exchange in the surface water export of metal, carbon and nutrient from the wetland.

Surface water

Fieldwork was carried out from 16 - 20 July 2018 at the site with surface water sampling starting at 12:00 pm on the first day. Samples were collected every hour for a total of 25 hrs continuously over two tidal cycles. Samples were taken with polypropylene syringes, filtered through 0.45 μm cellulose acetate filters and collected into 60 ml falcon tubes for dissolved carbon and nutrient analysis and 10 ml polypropylene acid washed vials for metals. Samples were collected and maintained following standard sampling methods detailed elsewhere (Holloway et al., 2016; Rutlidge et al., 2014).

Radon concentrations in water were measured using an automated radon-in-air detector modified to measure radon in water (RAD7, Durridge Co.) (Burnett et al., 2001; Peterson et al., 2019). Surface water was continually pumped at a rate of ~ 3 L/min from the middle of the creek into a gas equilibration device (GED), where the gas was circulated through a closed loop system via Drierite, as a desiccant, and into the RAD7. Radon concentrations were measured every 30 min with uncertainties ranging from 10% at low tide to 60% at high tide. A 30 min lag time correction, which is required for radon to reach equilibrium using this approach, was applied to the data (Dimova et al., 2009). Radon solubility was calculated as a function of temperature and salinity (Schubert et al., 2012).

Surface water physico-chemical parameters were measured using a calibrated YSI EXO_2 water quality multiparameter sonde. Variables including pH (±0.1 units), conductivity (±0.001 mS/cm), salinity (±0.1), dissolved oxygen (DO) (±0.1 mg/L), water temperature (±0.01 °C) and depth (±0.004 m) were collected at 15-min intervals. Fluorescent dissolved organic matter

(fDOM) concentrations were also measured using the same sonde and was used as a proxy for dissolved organic matter in the wetland water column. Wind speed data (±10%) was collected onsite using a weather station (Model PH1000). Current velocity and direction were measured in the channel using a Sontek Argonaut acoustic doppler current profiler (ADCP) at 15 min intervals.

Porewater

A total of 12 porewater samples were collected at different depths from the intertidal mudflat zones during the field campaign. Piezometers were installed via a hand auger up to 1.5 m deep using 50 mm PVC pipes. A peristaltic pump was used to collect samples after purging the bores three times. The porewater sampling procedure for dissolved material was similar to surface water after extracting porewater from the bores. The sampling approach applied here integrates the concentration of trace metal, carbon and nutrient in the upper 1.5 m of the soil where observed crab burrows increase the soil permeability. This approach permits characterisation of the porewater endmember that is more likely to discharge into and exchange with the surface water. Porewater physico-chemical characteristics such as DO, pH, EC and temperature were measured following established protocols using a handheld calibrated Hach Probe and through a flow cell system (Rutlidge et al., 2014). To measure radon in porewater samples, 6L gas-tight Nalgen HDPE bottles were used. Each bottle was connected to a RAD7 radon monitor device and given a minimum of 2 hrs to achieve an air-water radon equilibrium with <5% uncertainty (Lee and Kim, 2006).

Radon diffusion from sediments and ingrowth

Radon molecular diffusion from sediments was determined by collecting three sediment core samples from the study site. Each sample was placed in a gas-tight container with known dimensions, incubated with radium free water and sealed for at least one month. This approach is based on the radioactive properties of radon, where after six radon half-lives (~ 23 d), the source of the radon will reach equilibrium with the only sink (decay) within the core (Santos and Eyre, 2011). Water is then extracted from the container and collected into 6L gas-tight plastic bottles for radon measurements using a RAD7 as described above (Lee and Kim, 2006). The water column was sampled from bottom up to ensure mixing and prevent any effect of heterogeneity. Diffusion rates were used in the radon mass balance model and account for as a source of radon. To estimate radon ingrowth from its parent isotope (^{226}Ra), two 50L containers were filled with surface water at low and high tide. The water was then filtered through a

column containing 15-20 grs manganese oxide impregnated fibre which absorb ^{226}Ra (Moore, 2003). The fibres were then sealed and left for at least one month before ^{226}Ra concentration analysis following Kim et al. (2001) method.

Radon mass balance

A radon mass balance model was developed based on time series measurements following similar studies using this approach in tidal environments to estimate porewater exchange rates (Peterson et al., 2019). The mass balance considers all known radon sources (incoming flow, diffusion from sediments, ingrowth from parent isotopes and porewater inputs) and sinks (decay, outgoing flow and atmospheric evasion including wind- and current-driven evasion) and assumes the missing radon to balance the model is provided by porewater inputs in Equation (1):

$$Q_{gw}{}^{222}Rn_{gw} + Q_{in}{}^{222}Rn_{in} + Q_{dif}A + {}^{226}Ra\lambda_{222}V = Q_{out}{}^{222}Rn_{out} + {}^{222}Rn\lambda_{222}V + J_{atm/current}A \quad (1)$$

where Q_{gw} is the porewater exchange rate (m^3/s); $^{222}Rn_{gw}$ is the porewater endmember concentration (Bq/m^3); Q_{in} and $^{222}Rn_{in}$ are incoming flow (m^3/s) and radon concentration (Bq/m^3) during flood tide; Q_{dif} is radon diffusive flux (Bq/m^2/s); A is the surface area (m^2); ^{226}Ra is surface water radium concentration; λ_{222} is radon decay rate (0.181/d); V is the volume of water in the wetland; Q_{out} and $^{222}Rn_{out}$ are outgoing flow (m^3/s) and radon concentration (Bq/m^3) during ebb tide; $J_{atm/current}$ is radon atmospheric/current evasion (Bq/s).

Radon evasion losses were calculated based on an empirical equation that relates radon air-water concentration gradients, solubility (as a function of temperature and salinity), and gas transfer velocity following established gas exchange equations for tidal environments (MacIntyre et al., 1995; Borges et al., 2004).

$$J_{atm/current} = k\left({}^{222}Rn_w - \alpha{}^{222}Rn_{air}\right) \text{ A} \quad (2)$$

where $^{222}Rn_w$ and $^{222}Rn_{air}$ represent the radon concentration in water and air, respectively; α is the Ostwald solubility coefficient (dimensionless) describing the distribution of radon at equilibrium as the fluid to-gas ratio; and k is the gas transfer velocity at the air-water boundary (m/d). In tide-dominated waters, radon evasion is governed by wind, current and water depth. Therefore, gas transfer velocity (k) driven by wind, current and depth was estimated following equations from Borges et al. (2004) and MacIntyre et al. (1995) which have been well described

in previous studies (Sadat-Noori et al., 2016c; Santos et al., 2012b). The area of the entire wetland was used to upscale wind evasions, however, only the creek area was used to determine current-driven evasions as currents in the intertidal mudflats approached zero.

Analytical Analysis

Dissolved trace metal concentrations of Fe and Mn for both surface water and groundwater were analysed using a Perkin Elmer NexION 300D Inductively Coupled Plasma Mass Spectrometry (ICP-MS; Element II, Thermo-Fisher). Total dissolved phosphorous was measured using the ICP-MS instrument. Total dissolved nitrogen was measured using a Multi N/C analyser and an iTOC analyser was used for carbon analyses. All samples were analysed at the University of New South Wales (UNSW, Sydney) analytical centre following standard laboratory procedures.

Calculations

Wetland area and volume were measured in GIS using a digital elevation model (DEM) of the area. The uncertainty of the radon mass balance was calculated based on error propagation rules (Sadat-Noori et al., 2015). The standard deviation of the porewater radon and solute concentrations were used as the error for the porewater endmember. Porewater-derived fluxes were estimated by multiplying porewater exchange rates, calculated from the radon mass balance, by the median concentration of dissolved material in porewater. The median values are used here, rather than average values, as the data did not follow a normal distribution. Wetland solute export (ebb tide) and import (flood tide) was determined by multiplying hourly water flow rates by the time specific solute concentrations in the water column. Thereafter, export and import rates were integrating over a diel cycle (two tidal cycles) to calculate daily net export or import rates.

Results

Surface water time series observations

The area received a total of 5.5 mm of rainfall in the two weeks prior to the sampling campaign. With persistent dry conditions, the tidal forcing had a clear influence on many surface water physico-chemical parameters. The tidal range was 1.5 m and water depth in the creek varied between 0.2 to 1.7 m during the observed diurnal tides (Figure 2A). Electrical

Conductivity (EC) ranged from 44 to 57 mS/cm and decreased on ebb tides, although mainly staying within oceanic water concentrations (Figure 2C). Water temperature varied between 8 to 15 °C and showed a similar trend to EC variations, lowering at ebb tides. Median dissolved oxygen was 90 ± 13 % saturation with lower concentrations observed at ebb tide (Figure 2E). DO was supersaturated during the daytime of the first tidal cycle due to photosynthesis of phytoplankton in the presence of sunlight (Cui and Chui, 2019) and aeration caused by turbulence in the incoming flow (Figure 2B). pH ranged from 7.8 to 8.2 and followed the tidal trend with a clear decrease observed during ebb tides (Figure 2F). Radon concentrations varied from 60 to 260 Bq/m^3 and followed a reverse tidal trend with the highest concentrations observed during ebb tides (Figure 2H). Wind speed at the site ranged from 0 to 9.5 m/s (Figure 2G). fDOM concentrations were low at flood tide and increased at ebb tide, ranging from 8 to 71 QSU (Figure 2I).

Dissolved trace metal, carbon and nutrient in surface waters

Dissolved Fe and Mn had similar trends but were opposite to the tidal trend (highest concentrations at ebb tide) and similar to the observed radon trends (Figure 2J, K). Total dissolved Fe concentrations ranged from 0.03 μM at flood tide to 2.5 μM at ebb tide, whereas dissolved Mn concentrations varied between 0.2 to 1.4 μM. TDP and TDN had median concentrations of 3.3 ± 0.5 and 13.4 ± 8.4 (±1 SD) μM, respectively, with higher TDN concentrations during ebb tides (Figure 2L, M). TDP had an opposite trend to TDN, with higher concentrations during flow tide. Surface water TDN:TDP was higher at ebb tide and had a median value of 5.7 indicating N-limiting conditions in wetland surface water (Figure 2N). DOC and DIC had median concentrations of 40.7 ± 15.3 and 1756.8 ± 195.6 μM and both peaked at ebb tide (Figure 2O, P). However, DOC concentrations peaked almost 3 times higher on the first ebb tide compared to the second ebb tide. DIC had a clear peak on the first ebb tide but the peak was not as apparent on the second ebb tide.

Porewater observations

Porewater observations and analysis results are presented in Table 1. Median pH (6.9 ± 0.3) and DO (2.8 ± 2.1 mg/L) in porewater were lower than surface water observations (pH, 8.1 ± 0.2; DO 10.1 ± 2.6 mg/L), while porewater had a higher median temperature (17.1 ± 2.9 °C) than surface water (12.0 ± 2.1 °C). Porewater was hypersaline with a median EC of 72.0 ± 4.1 mS/cm, which was higher than surface water median EC concentration (51.7 ± 3.4 mS/cm). Median radon concentration in porewater (475 ± 203 Bq/m^3) was 3.5-fold higher than surface

water radon concentration. Median concentrations of Fe and Mn in porewater were over two orders of magnitude higher than surface water concentrations. Median porewater DOC and DIC concentrations were 4 and 14-fold higher than those observed in surface water, respectively. Median porewater TDN concentration was 9-fold higher than surface water, while similar median TDP concentration was observed in both porewater and surface water. Higher TDN concentrations in porewater resulted in a median TDN:TDP ratios of 48.5.

Radon mass balance model

The radon mass balance model revealed that tidal flow out of the system was the major radon loss accounting for over 86% of total radon losses (Table 2). From the remaining 14% of total losses, wind evasion accounted for ~13% and current evasion and radon decay accounted for 1%. The return flow from tidal waters during flood tide represented an important radon source to the wetland. However, these concentrations were of the same order of magnitude of radon losses during ebb tide. Molecular diffusion rate from wetland sediments was small (1.0 ± 0.2 Bq/m^2/day) and accounted for less than 1% of all radon sources.

The missing radon source to balance the equation was assumed to be porewater exchange and was estimated by dividing the missing radon flux by the radon porewater endmember concentration (474.9 ± 58.8 Bq/m^3). This resulted in a volumetric porewater exchange rate of 0.18 ± 0.08 m^3/s over the two tidal cycles. Considering the wetland area (112,450 m^2), porewater exchange rate was estimated to be 14.0 ± 6.3 cm/d on an areal basis (Table 2).

Wetland lateral exports

Wetland exports of dissolved Mn, Fe, TDN, TDP, DOC and DIC were estimated by multiplying individual solute observations by time specific surface water discharge rates and then integrating over the diel cycle to obtain a net export of solute from the wetland to the adjacent estuarine river system (Table 3). Overall, the wetland was a net exporter of Mn, Fe, TDN and DOC and a net importer for TDP and DIC (see negative fluxes in Table 3) despite porewater supplying these materials to the wetland surface water column. Surface water flow measured over the sampling period, showed that water was imported to the wetland from the adjacent river estuary.

Discussion

Porewater exchange rate and drivers

The radon observations at the site revealed a clear trend that can be best explained by porewater exchange. Other sources of radon such as molecular diffusion and ^{226}Ra decay represented a minor source, which is commonly observed in intertidal systems (Burnett et al., 2006; Peterson et al., 2008b; Santos et al., 2015; Santos et al., 2010; Swarzenski, 2007). The majority of the porewater estimated through the radon mass balance represents recirculated seawater. As illustrated by radon patterns in surface water over the sampling period (higher radon concentration observed at ebb tide; Figure 2H), and also a strong negative correlation between surface water radon concentrations and water depth (Figure 3), it is suggested that the main driver of porewater exchange at the site is tidal pumping. The site had a large number of crab burrows that may facilitate the porewater exchange process within mudflats zones through tidal pumping (Stieglitz et al., 2013; Xin et al., 2009). Therefore, it is expected that surface water infiltrates into sediments through the crab burrows at flood tide, accumulates a radon signal and discharges back out to the surface water column during ebb tide due to the hydraulic gradient of surface and groundwater.

The inverse relationship between surface water radon and EC (Figure 3) may indicate a freshwater radon source however, this is unlikely due to the small catchment size, flat topography and no upstream freshwater inputs at the site. The variation in surface water EC more likely represents a mixture of saline ocean water, river and porewater. Porewater EC were hypersaline (Table 1) and higher than surface water EC indicating high evaporation and no direct freshwater input to the system. Porewater samples were collected across the mudflats and in the upper reaches of the wetland, where water flushing and turnover times from the tide is less frequent (Bouillon et al., 2007b; Marchand et al., 2004). These processes will likely result in variations of porewater EC at the creek entrance of the wetland, versus within the mudflat areas of the wetland, and may explain the observed decrease in EC with decreasing water levels at ebb tide (Figure 2A, C). This likely explains the inverse relationship between radon and EC in surface water. Additionally, radon in porewater had a positive correlation with porewater EC, indicating that the source of radon is mostly saline porewater (Figure 3). Other studies have also reported a decrease in EC with decreasing water levels in mangrove tidal creek/estuaries where the source of radon was recirculated seawater (David et al., 2018; Taillardat et al., 2018). In future studies, combining radon and radium isotope measurements may help better quantify possible sources of porewater to the system.

Previous studies have reported porewater exchange rates ranging from 2.1 to 36 cm/d in mangroves creek, estuarine and intertidal systems using radon and radium isotope mass balance approaches (Chen et al., 2018; Stieglitz et al., 2013; Tait et al., 2017). Mangroves are known to be hotspots for porewater exchange processes and can have large porewater exchange rates (Gleeson et al., 2013; Xin et al., 2009). For example, in a recent study in eastern Australia (Coffs Harbour Estuary), Sadat-Noori et al. (2017) used radium isotopes to estimate average porewater exchange rates of 20.7±3.7 cm/d, while showing porewater exchange rates were higher in parts of the estuary where mangroves dominated the estuary. In another study, Tait et al., (2017) quantified porewater exchange rates using radon time series measurements in six tidal mangrove creeks in Australia (average 16.2 cm/d) and concluded that mangrove sites have higher porewater exchange rates compared to sites with other vegetation such as saltmarsh. Additionally, Gleeson et al. (2013) used radium measurements in a mangrove dominated tidal estuary (Moreton Bay, Australia), and reported an average porewater exchange rate of 17 cm/d, similar to porewater exchange rates estimated here (14.3 ± 1.3 cm/d). Nonetheless, the porewater exchange estimates provided in this study are within the broad range of previously reported mangrove porewater exchange rates.

The porewater exchange rate heavily depends on the radon endmember concentration in porewater which is usually considered as the main source of uncertainty when using radon as a natural geochemical groundwater tracer (Dulaiova and Burnett, 2008; Schmidt et al., 2010). This is because radon concentrations can vary by orders of magnitude within small spatial scales (Dulaiova et al., 2008; Smith et al., 2008). Here, porewater radon endmember concentrations did not vary significantly as the ratio between maximum and minimum concentrations was small (4) and the uncertainty for porewater radon samples was 12% (Table 1). The median radon porewater endmember was used to estimate the porewater exchange rates assuming our sample size (n=12) was reasonable relative to the catchment size. The final porewater exchange rate resulted in an uncertainty of 45%, which is in the lower range (23% - 120%) reported from previous studies using a radon mass balance approach (Peterson et al., 2008a; Sadat-Noori et al., 2015). This uncertainty was propagated into the porewater-derived solute fluxes using the standard deviation of porewater solute concentrations.

Wetland surface water trace metal, carbon and nutrient fluxes

Based on the measured water flow entering (flood tide) and leaving (ebb tide) the wetland over the two tidal cycles, the wetland was a net importer of water. Previous studies have also

reported higher water import than export in tidal mangrove environments with similar diurnal tidal trends (Michot et al., 2011; Taillardat et al., 2018). This import bias is a result of the tidal range difference observed between the two tidal cycles over the duration of the measurements. The first tidal cycle had a tidal range of 1.18 m, whereas the second tidal cycle had a tidal range of 1.40 m. The wetland was a net source (exporter) of Mn, Fe, TDN and DOC due to the higher solute concentration during ebb tides when water was leaving the system and porewater discharge was occurring.

The wetland exported 4.0 ± 0.6 and 6.6 ± 1.6 mmol/m^2 wetland/d (or 1.9 ± 0.4 and 3.2 ± 0.8 mmol/m^2 of catchment/d) of Mn and Fe, respectively, to the adjacent river estuary. Surface water export rates of Mn and Fe are limited in the literature, thereby the results of this study are compared to previously reported surface water Mn and Fe exports from mangroves, saltmarshes, estuaries and coastal bays to put the results into perspective (Table 4). It was observed that the estimated Fe and Mn exports in this study were higher than those observed previously in the literature. This is related to the specific characteristics of the study area. For example, the 2- and 3-fold higher Fe and Mn flux observed here compared to Fe and Mn flux reported for a subtropical estuary (Hat Head, Australia) draining a coastal wetland (Sanders et al., 2015), is likely due to Hat Head having sandy sediments whereas the system in this study had clay to silty sediments with strong iron content. Furthermore, the small catchment size, shallow depth and shorter residence time of water at the current study site contribute to higher fluxes. It is also suspected that the underlying potential acid sulfate soil at our study site plays an important role in the high concentration of porewater Fe and Mn and consequently higher export rates estimated here compared to previous studies.

Surface water TDN export was 11.2 ± 2.2 mmol/m^2 catchment/d which falls within the broad range of TDN export reported previously in the literature. Fluxes here were ~ 5-fold higher than the average TDN flux from multiples (tropical to temperate) mangrove creeks in Australia. The higher fluxes here are related to the distinctly high TDN concentrations in the porewaters of the study site likely due to nitrogen fixation by mangroves and oxidation of ammonia or ammonium to nitrate when sufficient oxygen is available in the sediment (Roé-Sosaa et al., 2019). Additionally, the high inputs of porewater-derived TDN to surface water plays a significant role in surface water TDN export at this site. A net surface water import of TDP was observed at our site which is consistent with previous studies in tidal mangrove environments (Gleeson et al., 2013; Tait et al., 2017).

Dissolved organic carbon accounted for 4% of the total dissolved carbon pool in the system. Global mangrove DOC export is estimated to be 2.2×10^{12} mol C per year (Dittmar et al., 2006) or 34.4 mmol/m^2/d based on the global area covered by mangroves ~1.6×10^{11} m^2 (Adame and Lovelock, 2011). The surface water DOC export here was 6-fold higher than the global mangrove DOC export estimation. In comparison to the literature on a catchment area basis, our DOC export estimates (88.9 ± 18.5 mmol/m^2/d) are higher than those reported from tropical and subtropical mangrove estuarine environments. Here, the source of DOC is expected to be from the mangrove vegetation as mangroves have the capacity to export ~50% of their net primary production as organic matter (Jennerjahn and Ittekkot, 2002) and have been identified as a major source of dissolved organic carbon to the oceans (Dittmar et al., 2006). Additionally, the high concentration of carbon in porewater and the active porewater exchange rates at the site was an important contributor to the high surface water DOC exports at this site.

The contribution of porewater exchange to surface water fluxes

Radon concentrations and the measured solute in porewater samples were significantly higher than surface water concentrations, indicating porewater exchange is likely a source of these material to surface water in this study (Figure 4). Additionally, the existing positive correlation between radon, Mn, Fe, TDN, DOC and fDOM, implies that the discharge of porewater with low pH, DO and high fDOM, Mn, Fe, TDN and DOC concentrations during low tide, is the major driver of dissolved material in this system (Figure 5H, G, F, C and A, respectively). These observations are consistent with a number of previous studies investigating porewater exchange in tidal mangrove creeks, which report a positive relationship between porewater discharge and solute concentrations in the water column (Bouillon et al., 2007a; Dittmar and Lara, 2001; Holloway et al., 2016; Pierre et al., 2018).

The radon mass balance provided stronger evidence and revealed a high porewater input of trace metal, carbon and nutrient to the wetland water column. Porewater-derived Mn was estimated to be 3.9 ± 1.1 mmol/m^2/d and contributed to 95% of Mn surface water export from the wetland. Porewater-derived Fe flux was 149.9 ± 56.7 mmol/m^2/d, which accounted for >100% of the surface water Fe exports. This inconsistency indicates that the Fe was oxidised, precipitated and/or flocculated at the sediment-water interface before leaving the system at low tide. Observations of a black ooze onsite, with a distinctive strong smell while collecting porewater samples, suggested the formation and precipitation of Fe-rich monosulfide black oozes (MBO) in the area which forms due to sulfate reduction in the presence of high Fe

concentrations (Table 1). These conditions are typical in acid sulfate soils on the eastern coast of Australia (Bush et al., 2004) and have been observed previously in subtropical and temperate mangrove wetlands (Holloway et al., 2018; Santos et al., 2011). The contribution of porewater-derived TDN (21.3 ± 5.5 mmol/m^2/d) and DOC (107.3 ± 28.5 mmol/m^2/d) to surface water exports were ~90 and 54%, respectively. Overall, these fluxes demonstrate the significant role of porewater exchange in transporting trace metal, carbon and nutrient from mangrove wetlands to coastal waters.

A limitation with our approach is that wetland fluxes presented here do not consider the effect of seasonal variability (rainfall), spring-neap tide cycles and tidal variability which may influence porewater exchange rates and consequently fluxes (Call et al., 2015; Oehler et al., 2018). Previous studies have reported higher porewater exchange rate in wet conditions compared to dry, in coastal wetland and estuarine systems (Jeffrey et al., 2016; Sadat-Noori et al., 2015). Here, as sampling was carried out in dry conditions, we interpret the calculated fluxes as conservative estimates and expect an increase in porewater-derived fluxes in wet conditions. However, more sampling is required to fully understand the responses and variations of the system in different environmental conditions.

While emphasising that porewater-derived dissolved metal, carbon and nutrient fluxes from temperate mangrove wetlands are limited worldwide, we provide a comprehensive comparison of estimated porewater-derived solutes with previous studies using natural traces (radon and radium isotopes) in coastal settings to relate our results to those found in other studies (Table 5). The porewater-derived Mn and Fe estimated from this study were greater than fluxes from mangroves and wetlands in the literature, (due to the small catchment size, existing underlying acid sulfate soils and high porewater solute concentrations), however, porewater-derived TDN, TDP and dissolved carbon fluxes are on the same order of magnitude and comparable to prior studies worldwide. The literature comparison highlights that temperate mangrove wetlands are an important source of solutes to rivers and coastal waters, with porewater exchange being a significant pathway for transportation.

Mangrove porewater solute flux vs river flux and its implications

The regional river estuary (Hunter River) in the area has an annual net surface water discharge of 3.4 m^3/s and average annual TDN, TDP and DOC concentrations of 31 ± 6, 1.4 ± 0.8 and 279 ± 17 μM, respectively. The lower catchment of Hunter River (Kooragang Island) covers 1,128 hectares of tidal mangrove wetlands with similar characteristics to the studied

wetland here (Brereton and Taylor-Wood, 2010). Since surface water exports from the mangrove wetland were estimated over a diel tidal cycle, and average EC level was indicative of oceanic values, it is assumed that no significant removal/transformation of material due to estuarine processes occurs and all dissolved material is exported to the ocean. Therefore, by upscaling our flux estimates to the entire mangrove area of the lower Hunter River catchment, mangrove porewater-derived TDN, TDP and DOC export to the coastal ocean was estimated to be at least 2 orders of magnitude higher annually, than those delivered via the river system. This highlights the necessity to account for mangrove porewater exchange in temperate mangrove wetlands, as a pathway for delivering carbon and nutrient to coastal waters.

The ratio of nitrogen to phosphorus (16:1) is an important factor that may control the primary productivity and the composition of the biological community in coastal waters (Redfield, 1934). Therefore, identifying and understanding the processes that drive N:P ratios is important. Here, surface water TDN:TDP values in the wetland changed from N-limiting to P-limiting conditions on the first ebb tide and significantly increased on the second ebb tide but remained under the Redfield Ratio (16:1 N:P) during measurements. This, in addition to the 9-fold higher median TDN:TDP ratios in porewater compared to surface water (Figure 4), suggests that porewater inputs of dissolved nitrogen during ebb tides (Figure 2A, M) may change the wetland, adjacent river estuary and the coastal waters to P-limiting conditions (Figure 2N). The positive relationship between the porewater tracer, radon, and TDN:TDP ratios (Figure 5D) further supports the possibility that porewater exchange can increase the TDN:TDP ratios of surface waters. Therefore, mangrove porewater exchange has the ability to alter and control wetland and estuary surface water nutrient ratios and should be accounted for in eutrophication management strategies. Previous studies have also reported the significant role of porewater exchange in nutrient dynamics within mangroves, wetlands, estuaries and bays (Gleeson et al., 2013; Sadat-Noori, et al., 2016b; Slomp and Van Cappellen, 2004).

Conclusion

In this study dissolved trace metal, carbon and nutrient exports from a small temperate mangrove-dominated tidal wetland were investigated and high export fluxes of Mn, Fe, TDN and DOC were estimated. Porewater exchange rate in the wetland was 14.0 ± 6.3 cm/d, indicating strong porewater dynamics in the channel and intertidal flats of the wetland. The multiple lines of evidence including higher concentrations of dissolved material in porewater

compared to surface water, positive correlation between radon and dissolved material, and flux calculations, indicated that porewater exchange was a major driver of Mn, Fe, TDN and DOC export from the wetland during our investigation. High fluxes of nitrogen inputs through porewater exchange was also a major regulator of surface water TDN:TDP ratios. Finally, mangrove porewater nutrient and organic carbon fluxes were found to rival those transported by the larger river system to the coastal ocean. This study shows that porewater exchange is a significant pathway for dissolved material input to surface waters and, as such, tidally influenced temperate mangrove wetlands with active porewater dynamics should be considered an important source of dissolved metal, carbon and nutrient to the coastal ocean.

Acknowledgments

We would like to thank Danial Khojasteh, Valentin Heimhuber and Shangqing Pei for their valuable assistance during the field campaign. We also appreciate the administrative and logistical support by Philip Reid and Hayley Ardagh from the Newcastle Coal Infrastructure Group (NCIG). Funding for this research was provided by the University of New South Wales (UNSW, Sydney) and Newcastle Coal Infrastructure Group which is hereby acknowledged.

Data Availability and Conflict of interest

All the data is available form the authors upon request. The authors declare no conflict of interest regarding this work.

Table 1. Porewater physico-chemical, radon, metal, carbon and nutrient observations.

Sample	Date	Depth (m)	EC (mS/cm)	Temp (°C)	pH	DO (mg/L)	Radon (Bq/m^3)	Fe (μM)	Mn (μM)	DOC (μM)	DIC (μM)	TDN (μM)	TDP (μM)	TDN:TDP
1	17/07/2018	1	72.7	18.3	6.6	1.6	418±50	923.4	48.7	534.8	3154.7	86.0	3.0	29.1
2	18/07/2018	0.8	75.8	16.7	6.5	2.7	689±96	3475.7	43.4	667.9	1568.0	117.8	2.8	41.8
3	17/07/2018	0.9	70	17.0	6.4	0.4	415±20	2451.4	27.9	1079.6	2792.5	188.9	2.8	66.6
4	18/07/2018	1.2	71.3	16.0	7.3	5.9	306±46	92.7	27.1	1130.5	9102.9	195.2	3.2	60.7
5	18/07/2018	0.9	78.1	17.0	7.0	3.4	393±100	798.3	19.4	864.3	8901.1	181.2	3.0	61.3
6	19/07/2018	0.8	74.9	10.7	7.1	4.8	564±117	2148.8	36.1	645.9	5556.1	142.5	3.1	45.3
7	19/07/2018	1.3	75.1	12.1	7.0	2.1	621±137	2297.4	35.7	1010.6	6010.8	195.9	3.3	59.2
8	19/07/2018	1.1	75.3	13.7	6.9	6.4	965±102	1216.8	32.4	925.6	7616.9	161.3	3.2	50.7
9	19/07/2018	0.8	71.2	16.9	6.8	5.7	401±16	657.4	14.3	406.4	5556.8	138.7	3.1	45.4
10	19/07/2018	0.7	62.7	17.9	7.2	0.5	232±41	759.6	11.9	608.3	19121.9	125.0	3.1	40.3
11	19/07/2018	0.8	71.1	19.9	7.0	2.8	332±41	1500.2	26.2	630.9	7875.6	137.2	3.0	45.9
12	19/07/2018	0.6	68	20.4	6.8	2.2	364±47	223.7	15.9	908.9	17664.6	171.4	4.9	35.2
	Median		72.0	17	6.9	2.8	475	1070.1	27.6	766.1	6813.8	151.9	3.1	48.5
	Std Dev		4.1	2.9	0.3	2.1	203	1020.8	11.6	232.1	5452.8	34.6	0.5	11.5
	Std Error		1.2	0.8	0.1	0.6	59	294.7	3.4	67.0	1574.1	10.0	0.2	3.3

Table 2. Results of the radon mass balance model and estimated porewater exchange rate in the wetland.

Mass balance terms	Symbol in Eq. (1)	Units	Radon flux	Contribution (%)
Volume	V	m^3		
Area	A	m^2		
Radon decay	$^{222}Rn\lambda_{222}V$	Bq/s	0.9 ± 0.1	0.2
Wind evasion	J_{atm}A	Bq/s	49.5 ± 12.1	12.7
Current evasion	$J_{current}$A	Bq/s	1.6 ± 0.6	0.4
Ebb tide outputs	$Q_{out}{}^{222}Rn_{out}$	Bq/s	338.3 ± 28.2	86.7
Total outputs		Bq/s	390.2 ± 30.7	100.0
Molecular diffusion	Q_{dif}	Bq/s	1.3 ± 0.5	0.4
^{222}Rn ingrowth from ^{226}Ra decay	$^{226}Ra\lambda_{222}V$	Bq/s	1.0 ± 0.4	0.2
Flood tide inputs	$Qin222Rnin$	Bq/s	301.3 ± 50.2	77.2
Missing (porewater)	$Q_{gw}{}^{222}Rn_{gw}$	Bq/s	86.6 ± 10.1	22.2
Total input		Bq/s	390.2 ± 43.3	100.0
Porewater exchange rate	Q_{gw}	m^3/s	0.18 ± 0.08	
Porewater exchange rate	Q_{gw}	cm/d	14.0 ± 6.3	

Table 3. Porewater-derived fluxes, areal and total wetland trace metal, carbon and nutrient exports. Porewater inputs were estimated by multiplying the radon-derived porewater exchange rate by the metal, carbon or nutrient porewater endmembers shown in Table 1. Negative values indicate net import into the wetland.

Solute	Porewater inputs ($mmol/m^2/d$)	Areal wetland export ($mmol/m^2/d$)	Total wetland export (kmol/year)	Porewater contribution (%)
Mn	3.9 ± 1.1	4.0 ± 0.6	166 ± 25	95
Fe	149.9 ± 56.7	6.6 ± 1.6	338 ± 51	>100
TDN	21.3 ± 5.6	23.9 ± 3.6	983 ± 147	89
TDP	0.4 ± 0.1	-10.1 ± 1.5	-415 ± 62	4
DOC	107.3 ± 29.1	197.7 ± 29.7	8113 ± 1217	54
DIC	954.5 ± 354.9	-5801.1 ± 908.0	-238,102 ± 35,768	15

Table 4. A comparison of surface water Mn, Fe, TDN and DOC export (mmol/m^2 of catchment/d) from wetlands, estuaries and intertidal areas from prior studies.

Location	System description	Catchment size (km^2)	Mn	Fe	TDN	DOC	Reference
Yaquina Estuary, USA	Temperate estuary	650	0.1 - 0.4				Callaway et al. (1988)
Western Port, Watson Inlet, Australia	Temperate mangrove coastal bay	4				25	Faber et al. (2014)
Tillamook Bay Estuary, USA	Temperate bay estuary	37	0.04				Colbert and McManus (2005)
Moreton Bay, Australia	Subtropical mangrove creek	4	0.6				Holloway et al., (2015)
Darwin, Australia	Tropical mangrove creek	7.3	0.2				
Tuckean Swamp, Australia	Subtropical wetland	400	0.01	0.1			Santos et al., (2011)
Hat Head, Australia	Subtropical estuary	18	0.01	1.4			Sanders et al., (2015)
Hat Head, Australia	Subtropical estuary	18				8.5	Sadat-Noori et al., (2016a)
Southern Moreton Bay, Australia	Subtropical mangrove tidal creek	0.4				25	Maher et al., (2013)
Southwest Florida coast, USA	Tropical mangrove estuary	230				41.1	Bergamaschi et al., (2012)
Hat Head, Australia	Subtropical estuary	18			46.7		Sadat-Noori et al., (2016b)
Multiple sites across Australia	Tropical to temperate mangrove creeks	38 - 360			2.4		Tait et al., (2016)
Waikareao, NZ	Intertidal mudflats	2.3			81.6		Santos et al., (2015)
Can Gio, Vietnam	Tropical tidal mangrove creek	0.5				44.5	Taillardat et al., (2018)
Kooragang Island, Australia	Temperate mangrove wetland	0.24	1.9	3.2	11.2	88.8	This study

Table 5. A comparison of porewater-derived (mmol/m^2/d) trace metal, carbon and nutrient fluxes from mangroves, saltmarsh, wetlands and mud flat systems.

Location	System	Porewater exchange rate (cm/d)	Porewater-derived Mn	Porewater-derived Fe	Porewater-derived TDN	Porewater-derived TDP	Porewater-derived DOC	Porewater-derived DIC	Reference
Kooragang Island, Aus.	Temperate mangrove wetland	14 ± 6	3.9 ± 1.1	149.9 ± 56.7	21.3 ± 5.5	0.4 ± 0.1	107.3 ± 28.5	954.5 ± 325.6	This study
Barwon Heads, Aus.	Temperate mangrove creek	8.0 ± 2.4		7.9					Holloway et al., 2018
Palma Beach, Balearic Islands, Majorca	Mediterranean bay	0.3		4.1					Rodellas et al. (2014)
Hat Head, Aus.	Subtropical estuary draining wetland	45.5 ±13	0.00003	0.001					Sanders et al. 2015
Tuckean swamp, NSW, Aus.	Subtropical acidy wetland	0.4	0.11	4.62					Santos et al. 2012
Barwon Heads estuary, Aus.	Temperate mangrove creek	8.0 ± 2.4			3.61 ± 1.49	0.16 ± 0.08			Tait et al. 2016
Waikareao, New Zealand	Temperate intertidal flats	27.1 ± 7.3			37.8	0.8			Santos et al. 2015
Western Port, Watson Inlet, Aus.	Temperate mangrove coastal bay	27 ± 2.6					0 - 25	130 - 450	Faber et al. 2014
Wadden Sea, Germany	Temperate intertidal flats	12			34–139		34–71		Santos et al. 2015
Darwin, Aus.	Tropical mangrove tidal creek	15.9	1.4						Holloway et al., 2016
Hinchinbrook Island, Aus.	Mild-tropical mangrove tidal creek	2.1	1.9						
Seventeen Seventy, Aus.	Subtropical mangrove tidal creek	35.5	0.2						
Moreton Bay, Australia	Subtropical mangrove tidal creek	24.9	1.2						
Matang Forest Reserve, Malaysia	Tropical mangrove forest	-	1.2						Alongi et al. (1998)
Moreton Bay, Aus.	Subtropical mangrove tidal creek	-					24	250	Maher et al. 2013
Okatee Estuary, USA	Mild-tropical salt marsh estuary	13.5					64	1079	Porubsky et al. (2014)
Okatee Estuary, USA	Mild-tropical salt marsh estuary	12.3					170	1960	Moore et al. (2006)
Hat Head, Aus.	Subtropical estuary draining wetland	45.5 ±13					540	687	Sadat-Noori et al. (2016)
Evans River, Aus.	Subtropical mangrove tidal creek	7.3					1941		Webb et al. (2018)
Moreton Bay, Aus.	Subtropical mangrove tidal creek	0.3			26.6	8.1			Gleeson et al., (2013)
Can Gio, Vietnam	Tropical tidal mangrove creek	5.1 ± 2.0					44.1	515	Taillardat et al., (2018)

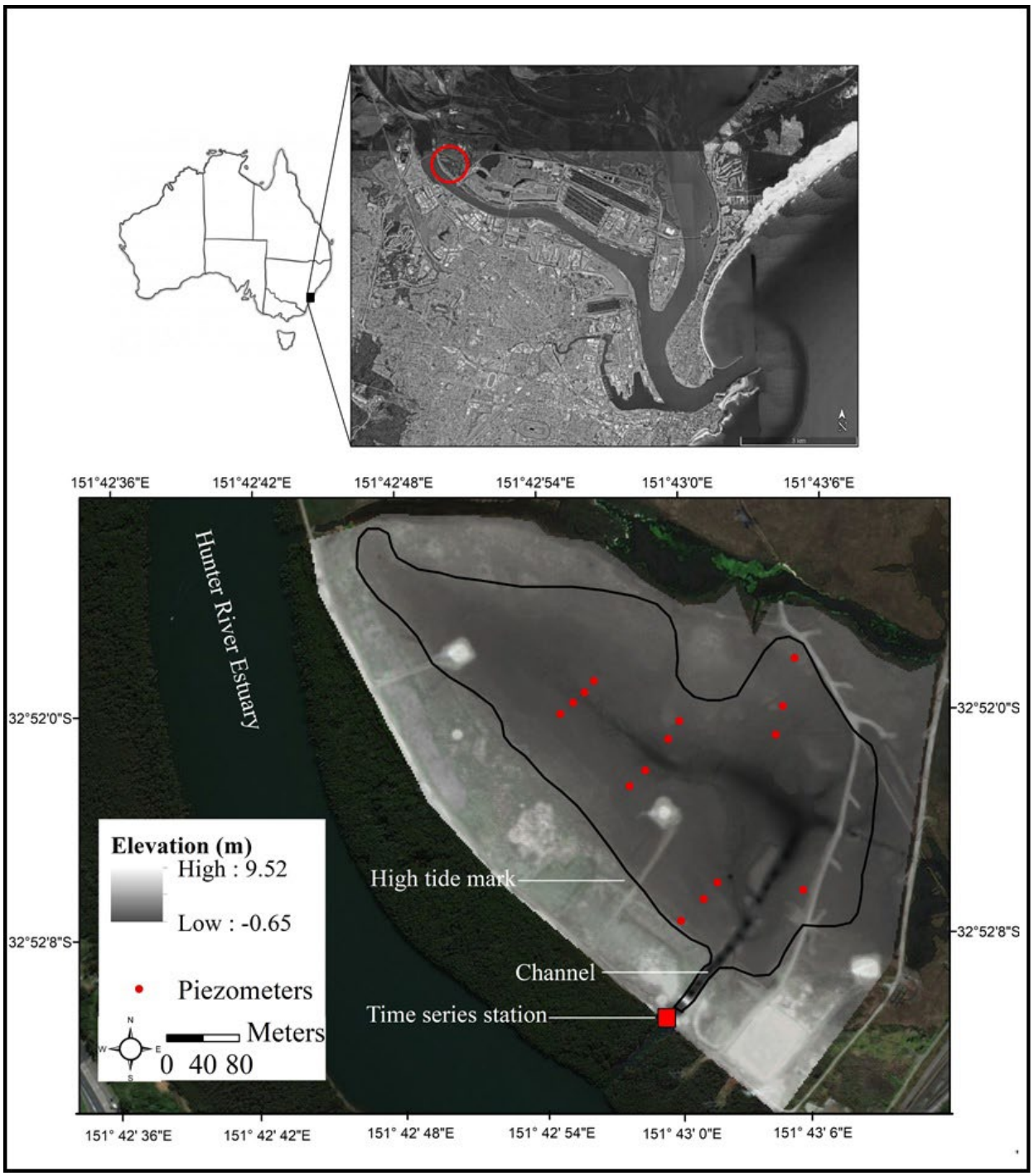

Figure 1. The map of the study area showing intertidal flats and the channel draining to Hunter River estuary. Red dots and the square indicate the location of porewater sampling and surface water time series measurements, respectively.

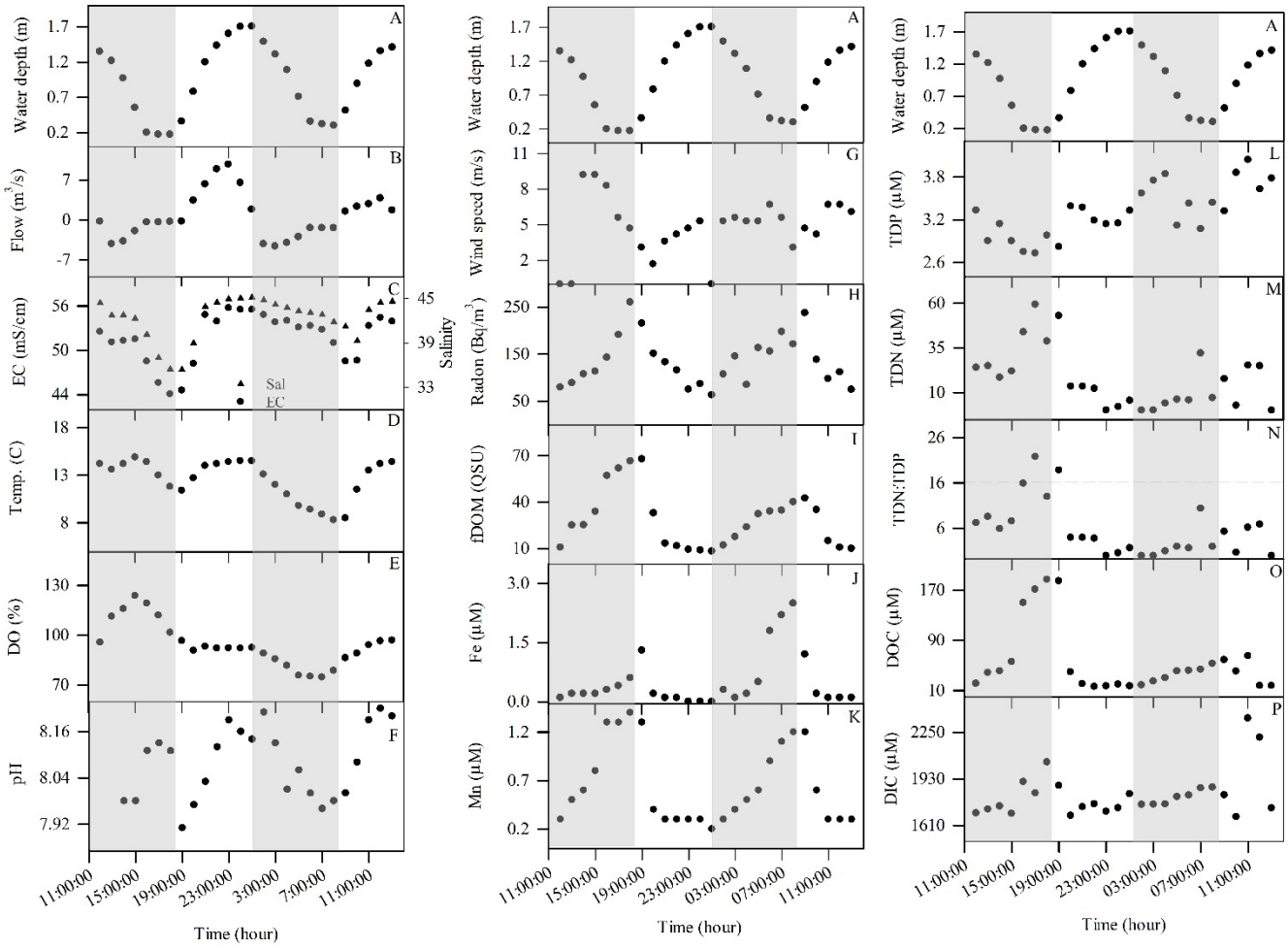

Figure 2. Surface water physico-chemical parameters, radon and dissolved solute concentration observations during time series measurements over two tidal cycles. Grey areas indicate outgoing tides.

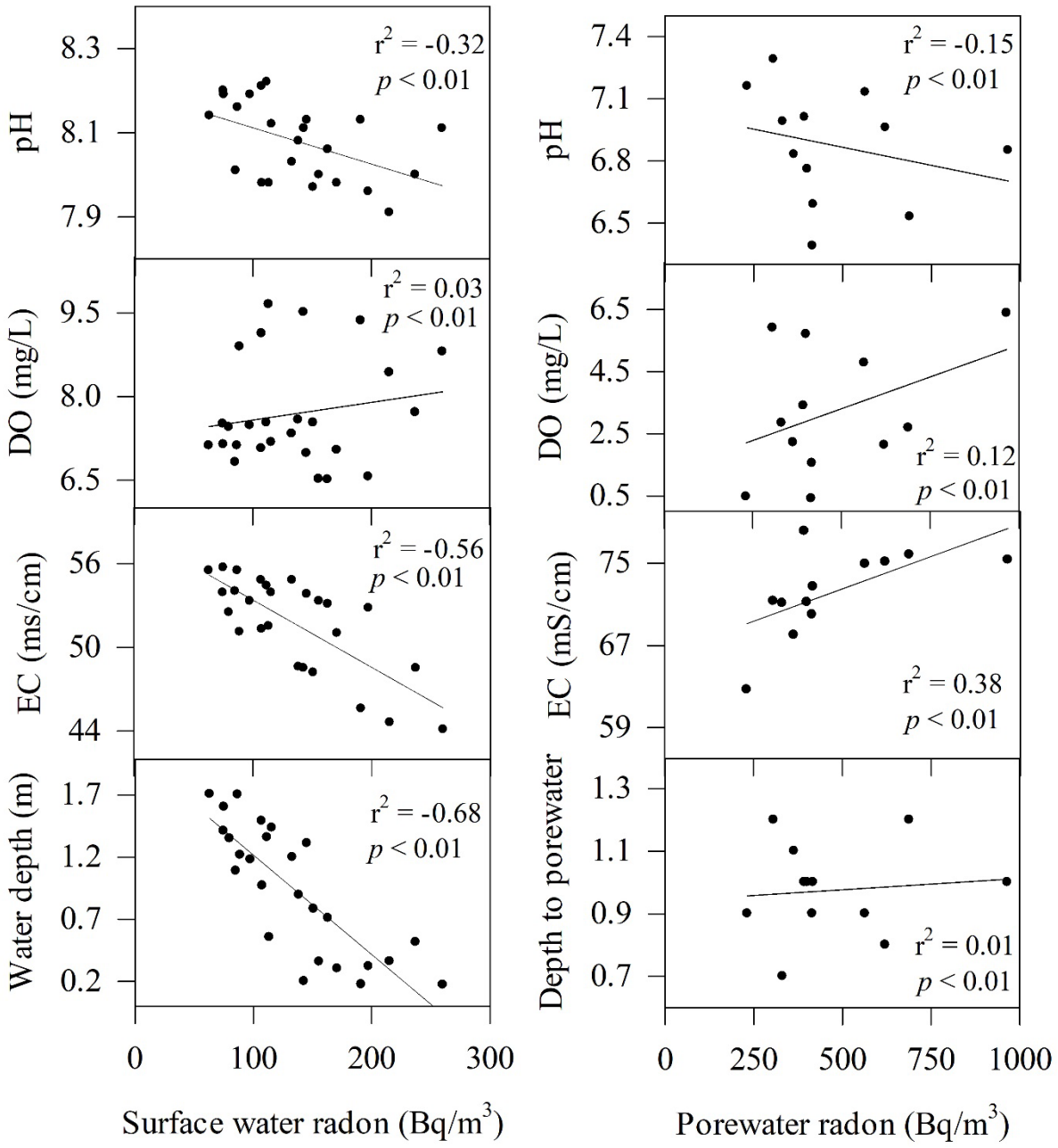

Figure 3. Surface water and porewater radon versus water depth, EC and pH scatter plots.

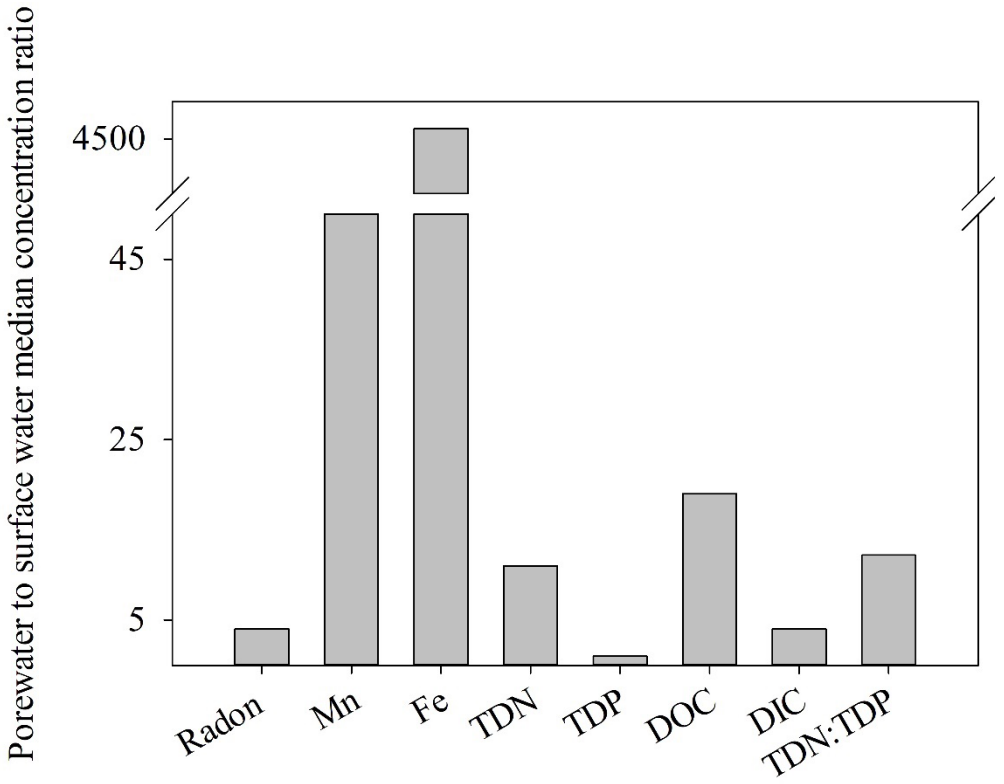

Figure 4. Ratio of median porewater to surface water radon and solute concentration.

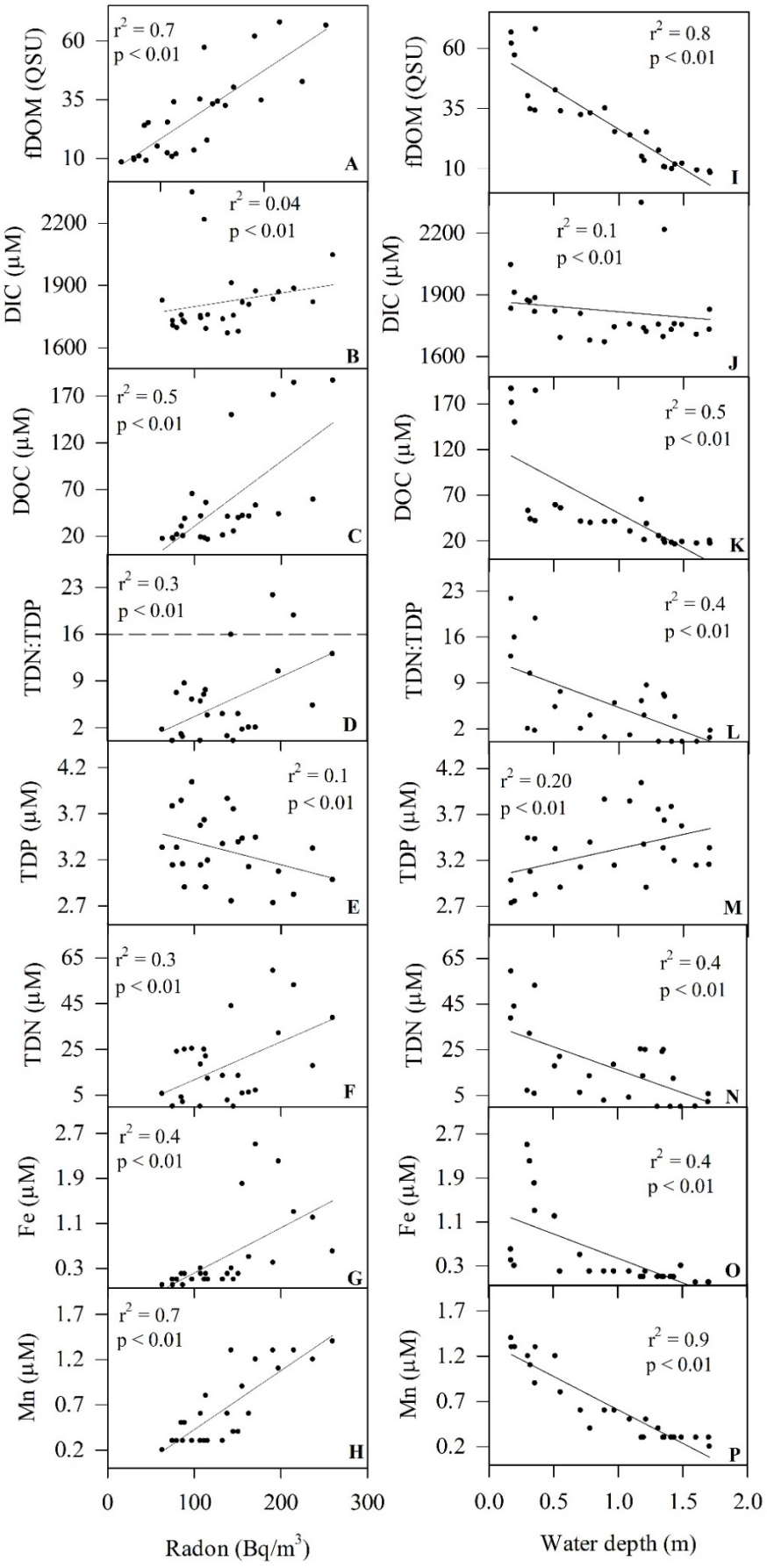

Figure 5. Radon and water depth correlation with metals, carbon and nutrients in surface water. Dashed line represents the Redfield ratio.

References

Adame, M.F., Lovelock, C.E., 2011. Carbon and nutrient exchange of mangrove forests with the coastal ocean. Hydrobiologia 663, 23-50.

Adyasari, D., Oehler, T., Afiati, N., Moosdorf N., 2019. Environmental impact of nutrient fluxes associated with submarine groundwater discharge at an urbanized tropical coast. Estuar. Coast. Shelf Sci. 221, 30-38.

Alongi, D., Sasekumar, A., Tirendi, F., Dixon, P., 1998. The influence of stand age on benthic decomposition and recycling of organic matter in managed mangrove forests of Malaysia. J. Exp. Mar. Biol. Ecol. 225, 197-218.

Bergamaschi, B.A., Krabbenhoft, D.P., Aiken, G.R., Patino, E., Rumbold, D.G., Orem, W.H., 2012. Tidally Driven Export of Dissolved Organic Carbon, Total Mercury, and Methylmercury from a Mangrove-Dominated Estuary. Environ Sci Technol. 46, 1371–1378.

Borges, A.V., Vanderborght, J.P., Schiettecatte, L.S., Gazeau, F., Ferrón-Smith, S., Delille, B., Frankignoulle, M., 2004. Variability of the gas transfer velocity of CO_2 in a macrotidal estuary (the Scheldt). Estuar. Coasts 27, 593-603.

Bouillon, S., Dehairs, F., Velimirov, B., Abril, G., Borges, A.V., 2007a. Dynamics of organic and inorganic carbon across contiguous mangrove and seagrass systems (Gazi Bay, Kenya). J. Geophys. Res. Biogeosci. 112, doi:10.1029/2006JG000325.

Bouillon, S., Middelburg, J.J., Dehairs, F., Borges, A.V., Abril, G., Flindt, M.R., Ulomi, S., Kristensen, E., 2007b. Importance of intertidal sediment processes and porewater exchange on the water column biogeochemistry in a pristine mangrove creek (Ras Dege, Tanzania). Biogeosci. Discuss. 4, 317-348.

Brereton, R., Taylor-Wood, E., 2010. Ecological Character Description of the Kooragang Component of the Hunter Estuary Wetlands Ramsar Site. Report to the Department of Sustainability, Environment, Water, Population and Communities (SEWPAC), Canberra, Australia.

Burnett, W., Kim, G., Lane-Smith, D., 2001. A continuous monitor for assessment of ^{222}Rn in the coastal ocean. J. Radioanal. Nucl. Chem. 249, 167-172.

Burnett, W.C., Aggarwal, P.K., Bokuniewicz, H., Cable, J.E., Charette, M.A., Kontar, E., Krupa, S., Kulkarni, K.M., Loveless, A., Moore, W.S., Oberdorfer, J.A., Oliveira, J., Ozyurt, N., Povinec, P., Privitera, A.M.G., Rajar, R., Ramessur, R.T., Scholten, J., Stieglitz, T., Taniguchi, M., Turner, J.V., 2006. Quantifying Submarine Groundwater Discharge in the Coastal Zone via Multiple Methods. Sci. Total Environ. 367, 498–543.

Burnett, W.C., Bokuniewicz, H., Huettel, M., Moore, W.S., Taniguchi, M., 2003. Groundwater and porewater inputs to the coastal zone. Biogeochem. 66, 3-33.

Burnett, W.C., Peterson, R., Moore, W.S., de Oliveira, J., 2008. Radon and radium isotopes as tracers of submarine groundwater discharge – results from the Ubatuba, Brazil SGD assessment intercomparison. Estuar. Coast. Shelf Sci. 76, 501-511.

Bush, R.T., Fyfe, D., Sullivan, L.A., 2004. Occurrence and abundance of monosulfidic black ooze in coastal acid sulfate soil landscapes. Soil Res. 42, 609-616.

Call M., Sanders, C. J., Macklin, P. A., Santos, I. R., Maher, D. T., 2019. Carbon outwelling and emissions from two contrasting mangrove creeks during the monsoon storm season in Palau, Micronesia. Estuar. Coast. Shelf Sci. 218, 340-348.

Call, M., Maher, D., Santos, I., Ruiz-Halpern, S., Mangion, P., Sanders, C., Erler, D., Oakes, J., Rosentreter, J., Murray, R., 2015. Spatial and temporal variability of carbon dioxide and methane fluxes over semi-diurnal and spring-neap-spring timescales in a mangrove creek. Geochim. Cosmochim. Acta. 150, 211-225.

Callaway, R.J., Specht, D.T., Ditsworth, G.R., 1988. Manganese and suspended matter in the Yaquina Estuary, Oregon. Estuar. 11, 217-225.

Chen, X., Zhang, F., Lao, Y., Wang, X., Du, J., Santos, I.R., 2018. Submarine groundwater discharge-derived carbon fluxes in mangroves: An important component of blue carbon budgets? J. Geophys. Res. Oceans. 123, 6962-6979.

Cho, H.M., Kim, G., Kwon, E.Y., Moosdorf, N., Garcia-Orellana, J., Santos, I.R., 2018. Radium tracing nutrient inputs through submarine groundwater discharge in the global ocean. Sci. Rep. 8, 2439.

Colbert, D., McManus, J., 2005. Importance of seasonal variability and coastal processes on estuarine manganese and barium cycling in a Pacific Northwest estuary. Cont. Shelf Res. 25, 1395-1414.

Cui, W., and Chu, T. F. M., 2017. Temporal variations in water quality in a brackish tidal pond: Implications for governing processes and management strategies. J. Environ.Manage. 193, 108-117.

David, F., Meziane, T., Tran-Thi, N.T., Truong Van, V., Thanh-Nho, N., Taillardat, P., Marchand, C., 2018. Carbon biogeochemistry and CO_2 emissions in a human impacted and mangrove dominated tropical estuary (Can Gio, Vietnam). Biogeochem. 138, 261-275.

David., M., Bailly-Comte, V., Munaron, D., Fiandrino, A., Stieglitz, T.C. 2019. Groundwater discharge to coastal streams – A significant pathway for nitrogen inputs to a hypertrophic Mediterranean coastal lagoon. Sci. Total Environ. 677, 142-155.

Diggle, R.M., Tait, D.R., Maher, D.T., Huggins, X., Santos, I.R. 2019. The role of porewater exchange as a driver of CO2 flux to the atmosphere in a temperate estuary (Squamish, Canada). Environ. Earth Sci. 78(11), 336.

Dimova, N., Burnett, W.C., Lane-Smith, D., 2009. Improved automated analysis of radon (^{222}Rn) and thoron (^{220}Rn) in natural waters. Environ. Sci. Technol. 43, 8599-8603.

Dittmar, T., Hertkorn, N., Kattner, G., Lara, R.J., 2006. Mangroves, a major source of dissolved organic carbon to the oceans. Global biogeochem. Cy. 20.

Dittmar, T., Lara, R., 2001. Driving forces behind nutrient and organic matter dynamics in a mangrove tidal creek in North Brazil. Estuar. Coast. Shelf Sci. 52, 249-259.

Dulaiova, H., Burnett, W.C., 2008. Evaluation of the flushing rates of Apalachicola Bay, Florida via natural geochemical tracers. Mar. Chem. 109, 395-408.

Dulaiova, H., Gonneea, M.E., Henderson, P.B., Charette, M.A., 2008. Geochemical and physical sources of radon variation in a subterranean estuary—implications for groundwater radon activities in submarine groundwater discharge studies. Mar. Chem. 110, 120-127.

Faber, P.A., Evrard, V., Woodland, R.J., Cartwright, I.C., Cook, P.L., 2014. Pore-water exchange driven by tidal pumping causes alkalinity export in two intertidal inlets. Limnol. Oceanogr. 59, 1749-1763.

Gleeson, J., Santos, I.R., Maher, D.T., Golsby-Smith, L., 2013. Groundwater–surface water exchange in a mangrove tidal creek: Evidence from natural geochemical tracers and implications for nutrient budgets. Mar. Chem. 156, 27-37.

Goodridge, B., 2018. The influence of submarine groundwater discharge on nearshore marine dissolved organic carbon reactivity, concentration dynamics, and offshore export. Geochim. Cosmochim. Acta. 241, 108-119.

Holloway, C.J., Santos, I.R., Rose, A.L., 2018. Porewater inputs drive Fe redox cycling in the water column of a temperate mangrove wetland. Estuar. Coast. Shelf Sci. 207, 259-268.

Holloway, C.J., Santos, I.R., Tait, D.R., Sanders, C.J., Rose, A.L., Schnetger, B., Brumsack, H.J., Macklin, P.A., Sippo, J.Z., Maher, D.T., 2016. Manganese and iron release from mangrove porewaters: A significant component of oceanic budgets? Mar. Chem. 184, 43-52.

Jeffrey, L.C., Maher, D.T., Santos, I.R., McMahon, A., Tait, D.R., 2016. Groundwater, acid and carbon dioxide dynamics along a coastal wetland, lake and estuary continuum. Estuar. Coasts 39, 1325-1344.

Jennerjahn, T.C., Ittekkot, V., 2002. Relevance of mangroves for the production and deposition of organic matter along tropical continental margins. Naturwissenschaften 89, 23-30.

Kim, G., Burnett, W., Dulaiova, H., Swarzenski, P., Moore, W., 2001. Measurement of 224Ra and 226Ra activities in natural waters using a radon-in-air monitor. Environ. Sci. Tech. 35, 4680-4683.

Lee, J.M., Kim, G., 2006. A simple and rapid method for analyzing radon in coastal and ground waters using a radon-in-air monitor. J. Environ. Radioact. 89, 219-228.

MacIntyre, S., Wanninkhof, R., Chanton, J., 1995. Trace gas exchange across the air-water interface in freshwater and coastal marine environments. Biogenic trace gases: Measuring emissions from soil and water, 52-97.

Maher, D.T., Santos, I.R., Golsby-Smith, L., Gleeson, J., Eyre, B.D., 2013. Groundwater-derived dissolved inorganic and organic carbon exports from a mangrove tidal creek: The missing mangrove carbon sink? Limnol. Oceanogr. 58, 475–488.

Marchand, C., Baltzer, F., Lallier-Vergès, E., Albéric, P., 2004. Pore-water chemistry in mangrove sediments: relationship with species composition and developmental stages (French Guiana). Mar. Geol. 208, 361-381.

Michot, B., Meselhe, E.A., Rivera-Monroy, V.H., Coronado-Molina, C., Twilley, R.R., 2011. A tidal creek water budget: Estimation of groundwater discharge and overland flow using hydrologic modeling in the Southern Everglades. Estuar. Coast. Shelf Sci. 93, 438-448.

Moore, W.S., 2003. Sources and fluxes of submarine groundwater discharge delineated by radium isotopes. Biogeochem. 75–93, 75–93.

Moore, W.S., 2006. The role of submarine groundwater discharge in coastal biogeochemistry. J. Geochem. Explor. 88, 389-393.

Moore, W.S., 2010. The effect of submarine groundwater discharge on the ocean. Annu. Rev. Mar. Sci. 2, 59-88.

Moore, W.S., Blanton, J.O., Joye, S.B., 2006. Estimates of flushing times, submarine groundwater discharge, and nutrient fluxes to Okatee Estuary, South Carolina. J. Geophys. Res. Oceans. 111.

Oehler, T., Eiche, E., Putra, D., Adyasari, D., Hennig, H., Mallast, U., Moosdorf, N., 2018. Seasonal variability of land-ocean groundwater nutrient fluxes from a tropical karstic region (southern Java, Indonesia). J. Hydrol. 565, 662-671.

Peterson, R.N., Meile, C., Peterson, L.E., Carter. M., Miklesh. D., 2019. Groundwater discharge dynamics into a salt marsh tidal river. Estuar. Coast. Shelf Sci. 218, 324-333.

Peterson, R.N., Burnett, W.C., Taniguchi, M., Chen, J., Santos, I.R., Ishitobi, T., 2008a. Radon and radium isotope assessment of submarine groundwater discharge in the Yellow River delta, China. J. Geophys. Res. 113, 9 - 21.

Peterson, R.N., Burnett, W.C., Taniguchi, M., Chenc, J., Santos, I.R., Misra, S., 2008b. Determination of transport rates in the Yellow River–Bohai Sea mixing zone via natural geochemical tracers. Cont. Shelf Res. 28, 2700–2707.

Pierre, T., Pim, W., Cyril, M., Daniel, A.F., David, W., Paul, B., Van Vinh, T., Thanh-Nho, N., Alan, D.Z., 2018. Assessing the contribution of porewater discharge in carbon export and CO_2 evasion in a mangrove tidal creek (Can Gio, Vietnam). J. Hydrol. 563, 303-318.

Porubsky, W.P., Weston, N.B., Mooreb, W.S., Ruppel, C., Joye, S.B., 2014. Dynamics of submarine groundwater discharge and associated fluxes of dissolved nutrients, carbon, and trace gases to the coastal zone (Okatee River estuary, South Carolina). Geochim. Cosmochim. Acta. 131, 81–97.

Redfield, A.C., 1934. On the proportions of organic derivatives in sea water and their relation to the composition of plankton. James Johnstone Memorial Volume, University Press of Liverpool, 176-192.

Rodellas, V., Garcia-Orellana, J., Tovar-Sánchez, A., Basterretxea, G., López-Garcia, J.M., Sánchez-Quiles, D., Garcia-Solsona, E., Masqué, P., 2014. Submarine groundwater discharge as a source of nutrients and trace metals in a Mediterranean bay (Palma Beach, Balearic Islands). Mar.Chem. 160, 56-66.

Roé-Sosaa, A., Rangel-Perazab, J.G., Rodríguez-Matac, A.E., Pat-Espadasd, A., Bustos-Terronesc, Y., Diaz-Peñab, I., Manh Vue, C., Amabilis-Sosac, L. E. 2019. Emulating natural wetlands oxygen conditions for the removal of N and P in agricultural wastewaters. J. Environ. Manage. 236, 351–357.

Rutlidge, H., Baker, A., Marjo, C.E., Andersen, M.S., Graham, P.W., Cuthbert, M.O., Rau, G.C., Roshan, H., Markowska, M., Mariethoz, G., 2014. Dripwater organic matter and trace element geochemistry in a semi-arid karst environment: Implications for speleothem paleoclimatology. Geochim. Cosmochim. Acta. 135, 217-230.

Sadat-Noori, M., Maher, D.T., Santos, I.R., 2016a. Groundwater Discharge as a Source of Dissolved Carbon and Greenhouse Gases in a Subtropical Estuary. Estuar. Coasts 39, 639-656.

Sadat-Noori, M., Santos, I.R., Sanders, C.J., Sanders, L.M., Maher, D.T., 2015. Groundwater Discharge into an Estuary Using Spatially Distributed Radon Time Series and Radium Isotopes. J. Hydrol. 528, 703-719.

Sadat-Noori, M., Santos, I.R., Tait, D.R., Maher, D.T., 2016b. Fresh meteoric versus recirculated saline groundwater nutrient inputs into a subtropical estuary. Sci Total Environ. 566, 1440-1453.

Sadat-Noori, M., Santos, I.R., Tait, D.R., McMahon, A., Kadel, S., Maher, D.T., 2016c. Intermittently Closed and Open Lakes and/or Lagoons (ICOLLs) as groundwater-dominated coastal systems: Evidence from seasonal radon observations. J. Hydrol. 535, 612-624.

Sadat-Noori, M., Santos, I.R., Tait, D.R., Reading, M.J., Sanders, C.J., 2017. High porewater exchange in a mangrove-dominated estuary revealed from short-lived radium isotopes. J. Hydrol. 553, 188-198.

Sanders, C.J., Eyre, B.D., Santos, I.R., Machado, W., Luiz-Silva, W., Smoak, J.M., Breithaupt, J.L., Ketterer, M.E., Sanders, L., Marotta, H., 2014. Elevated rates of organic carbon, nitrogen, and phosphorus accumulation in a highly impacted mangrove wetland. Geophys. Res. Lett. 41, 2475-2480.

Sanders, C.J., Santos, I.R., Maher, D.T., Sadat-Noori, M., Schnetger, B., Brumsack, H.J., 2015. Dissolved iron exports from an estuary surrounded by coastal wetlands: Can small estuaries be a significant source of Fe to the ocean? Mar. Chem. 176, 75-82.

Santos, I.R., Beck, M., Brumsack, H.-J., Maher, D.T., Dittmar, T., Waska, H., Schnetger, B., 2015. Porewater exchange as a driver of carbon dynamics across a terrestrial-marine transect: Insights from coupled ^{222}Rn and pCO_2 observations in the German Wadden Sea. Mar. Chem. 171, 10-20.

Santos, I.R., Bryan, K.R., Pilditch , C.A., Tait, D.R., 2014. Influence of porewater exchange on nutrient dynamics in two New Zealand estuarine intertidal flats. Mar. Chem. 167, 57-70.

Santos, I.R., De Weys, J., Eyre, B.D., 2011. Groundwater or floodwater? Assessing the pathways of metal exports from a coastal acid sulfate soil catchment. Environ. Sci. Technol. 45, 9641-9648.

Santos, I.R., Eyre, B.D., 2011. Radon tracing of groundwater discharge into an Australian estuary surrounded by coastal acid sulphate soils. J. Hydrol. 396, 246-257.

Santos, I.R., Eyre, B.D., Huettel, M., 2012a. The driving forces of porewater and groundwater flow in permeable coastal sediments: A review. Estuar. Coast. Shelf Sci. 98, 1- 15.

Santos, I.R., Maher, D.T., Eyre, B.D., 2012b. Coupling automated radon and carbon dioxide measurements in coastal waters. Environ. Sci. Technol. 46, 7685-7691.

Santos, I.R., Peterson, R.N., Eyre, B.D., Burnett, W.C., 2010. Significant lateral inputs of fresh groundwater into a stratified tropical estuary: evidence from radon and radium isotopes. Mar. Chem. 121, 37-48.

Schmidt, A., Gibson, J.J., Santos, I.R., Schubert, M., Tattrie, K., Weiss, H., 2010. The contribution of groundwater discharge to the overall water budget of two typical Boreal lakes in Alberta/Canada estimated from a radon mass balance. Hydrol. Earth Syst. Sci. 14, 79–89.

Schubert, M., Paschke, A., Lieberman, E., Burnett, W.C., 2012. Air-water partitioning of ^{222}Rn and its dependence on water temperature and salinity. Environ. Sci. Technol. 46, 3905-3911.

Slomp, C.P., Van Cappellen, P., 2004. Nutrient inputs to the coastal ocean through submarine groundwater discharge: controls and potential impact. J. Hydrol. 295, 64-86.

Smith, C.G., Cable, J.E., Martin, J.B., Roy, M., 2008. Evaluating the source and seasonality of submarine groundwater discharge using a radon-222 pore water transport model. Earth Planet. Sci. Lett. 273, 312–322.

Stieglitz, T., 2005. Submarine groundwater discharge into the near-shore zone of the Great Barrier Reef, Australia. Marine Pollut. Bull. 51, 51-59.

Stieglitz, T.C., Clark, J.F., Hancock, G.J., 2013. The mangrove pump: The tidal flushing of animal burrows in a tropical mangrove forest determined from radionuclide budgets. Geochim. Cosmochim. Acta. 102, 12-22.

Swarzenski, P., 2007. U/Th series radionuclides as coastal groundwater tracers. Chem. Rev. 107, 663-674.

Taillardat, P., Ziegler, A.D., Friess, D.A., Widory, D., Van, V.T., David, F., Thành, N.N., Marchand, C., 2018. Carbon dynamics and inconstant porewater input in a mangrove tidal creek over contrasting seasons and tidal amplitudes. Geochim. Cosmochim. Acta. 237, 32-48.

Tait, D.R., Maher, D.T., Sanders, C.J., Santos, I.R., 2017. Radium-derived porewater exchange and dissolved N and P fluxes in mangroves. Geochim. Cosmochim. Acta. 200, 295-309.

Thanh-Nho, N., Marchand, C., Strady, E., Vinhbe, T., Nhu-Trang, T., 2019. Metals geochemistry and ecological risk assessment in a tropical mangrove (Can Gio, Vietnam). Chemosphere, 219, 365-382.

Wang W., Sardans J., Wang C., Zeng C., Tong C., Chen G., Huang J., Pan H., Peguero G., Vallicrosa H., Peñuelas J., 2019. The response of stocks of C, N, and P to plant invasion in the coastal wetlands of China. Glob. Chang. Biol., 25, 733-743.

Webb, J.R., Santos, I.R., Maher, D.T., Tait, D.R., Cyronak, T., Sadat-Noori, M., Macklin, P., Jeffrey, L.C., 2019. Groundwater as a source of dissolved organic matter to coastal waters: Insights from radon and CDOM observations in 12 shallow coastal systems. Limnol. Oceanogr. 64, 182-196.

Xin, P., Jin, G., Li, L., Barry, D.A., 2009. Effects of crab burrows on pore water flows in salt marshes. Adv. Water Resour. 32, 439-449.

Zhou, Y., Sawyer, A. H., David, C. H., Famiglietti, J. S., 2019. Fresh Submarine Groundwater Discharge to the Near-Global Coast. Geophys. Res.Lett. https://doi.org/10.1029/2019GL082749